

Technical Note: Magnetometer Sensor and Calibration

Paul F. Roysdon[†]

Jay A. Farrell[‡]

I. INTRODUCTION

While excellent texts exist on the topic of magnetometers [1], and magnetic heading calculation [2], [3], the detailed discussion of calibration and tilt-compensation is not presented. This article summarizes the equations for three-axis magnetometer calibration, and calculation of the tilt-compensated magnetic heading with correction for true north. Two illustrative examples are provided to demonstrate sensor calibration, and heading calculation. This article assumes that the application is generic, and changes to the local magnetism are fixed, e.g. no magnetic fluctuation due to electric motors (a common source of error on small UAV's).

II. EARTH MAGNETIC FIELD

At any location on Earth, either at the surface or above it, the magnetic field can be locally represented as a constant three dimensional vector (\mathbf{h}_0). This vector is characterized by three properties. The first property is intensity, or magnitude (\mathcal{F}), which is normally measured in nano-Teslas (nT) with an approximate range of $25000nT$ to $65000nT$. Second, the inclination (\mathcal{I}), with negative values (up to -90°) if pointing up and positive (up to 90°) if pointing down. And finally the declination (\mathcal{D}), which measures the deviation of the field relative to the geographical (true) north and is positive eastward.

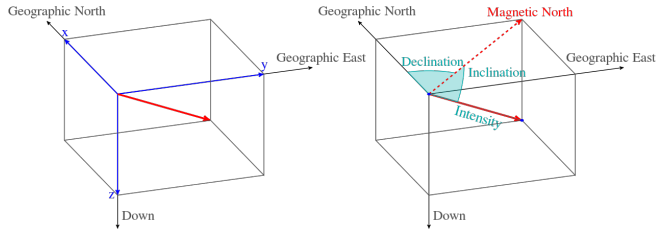


Fig. 1. Magnetic Field Components. [4]

Using the frame of reference in Fig. 1, the Earth magnetic field vector \mathbf{h}_0 is

$$\mathbf{h}_0 = \mathcal{F} \begin{bmatrix} \cos(\mathcal{I}) \cos(\mathcal{D}) \\ \cos(\mathcal{I}) \sin(\mathcal{D}) \\ \sin(\mathcal{I}) \end{bmatrix} \quad (1)$$

Given a geographical point the World Magnetic Model (WMM) [4] can be used to obtain the expected values for \mathcal{F} , \mathcal{I} and \mathcal{D} . The magnetic declination is necessary to calculate the geographical north from a compass. The WMM values for the current epoch (y.2015) are provided in the Appendix, see Figs. 12 - 18.

[†]Ph.D. student, [‡]Professor at the Dept. of Electrical & Computer Engineering, UC Riverside. {proysdon, farrell}@ece.ucr.edu.

III. MEASURING WITH A MAGNETOMETER

Assuming an ideal 3-axis magnetometer in an environment free of magnetic disturbance, a magnetometer reading \mathbf{h} taken with an arbitrary orientation (ϕ, θ, ψ) is

$$\mathbf{h} = \mathbf{R}_x(\phi) \mathbf{R}_y(\theta) \mathbf{R}_z(\psi) \mathbf{h}_0 \quad (2)$$

where \mathbf{h}_0 is the local Earth magnetic field given in eqn. (1) and $\mathbf{R}_x(\phi)$, $\mathbf{R}_y(\theta)$, $\mathbf{R}_z(\psi)$ are rotation matrices around the frame of reference x , y , z axis, respectively. Assume orientation is provided by external sources, e.g. and Inertial Measurement Unit (IMU). It is easy to see that multiple samples produce a sphere of radius \mathcal{F} :

$$\mathbf{h}^\top \mathbf{h} = \dots = \mathcal{F}^2. \quad (3)$$

The sphere is important because the 3D heading vector is calculated from the three components of the local magnetic field. Distortion of the sphere, e.g. an ellipsoid, results in a heading vector error, which is discussed in the following sections.

A simulated example of eqn. (3) is shown in Fig. 2.

Magnetometer Calibration Demo: True Data

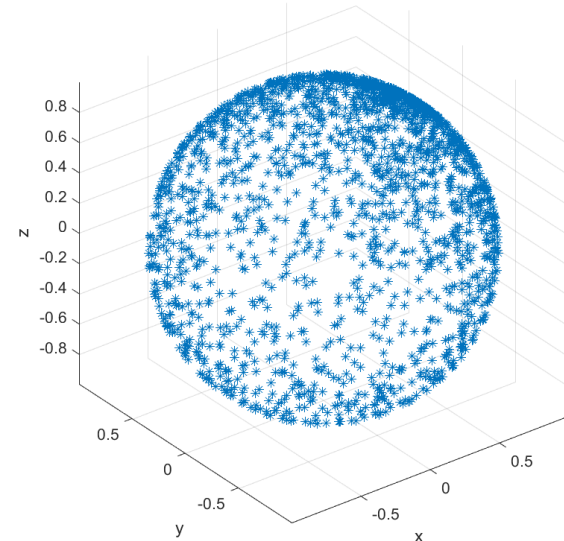


Fig. 2. Expected samples of a 3-axis magnetometer in Riverside, CA.

IV. DISTORTION SOURCES

There are two primary categories of measurement distortion sources [5]: instrumentation errors and magnetic interferences.

A. Instrumentation errors

Instrumentation errors are unique and constant for each sensor, and are modeled with three components. First, a scale factor, which is modeled as a diagonal matrix

$$\mathbf{S} = \begin{bmatrix} s_x & 0 & 0 \\ 0 & s_y & 0 \\ 0 & 0 & s_z \end{bmatrix}, \quad (4)$$

Second, the non-orthogonality of the sensor axis, which is modeled as

$$\mathbf{N} = [n_x \ n_y \ n_z]^\top, \quad (5)$$

where each column represents a vector of size three corresponding to each sensor axis with respect to the sensor frame. Finally, a sensor offset (bias) which is modeled as

$$\mathbf{b}_{so} = [b_{so_x} \ b_{so_y} \ b_{so_z}]^\top. \quad (6)$$

Fig. 3 presents a graphical representation of each instrumentation error axes, relative to the true axes.

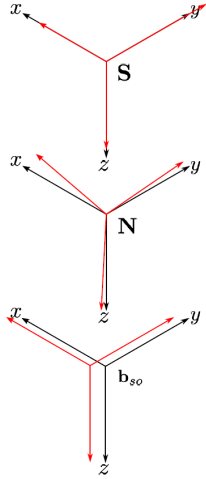


Fig. 3. Schematic representation of each instrumentation error.

B. Magnetic interferences

Magnetic interferences are caused by ferromagnetic elements present in the surroundings of the sensor, comprised of permanent (hard iron) and induced magnetism (soft iron). Note that we ignore any non-constant magnetic interference.

Hard iron results from permanent magnets and magnetic hysteresis, which is equivalent to a bias, modeled as

$$\mathbf{b}_{hi} = [b_{hi_x} \ b_{hi_y} \ b_{hi_z}]^\top. \quad (7)$$

Soft iron interference is the interaction of an external magnetic field with ferromagnetic materials, causing a change in the intensity and direction of the sensed field, modeled as

$$\mathbf{A}_{si} = \begin{bmatrix} a_{11} & a_{12} & a_{13} \\ a_{21} & a_{22} & a_{23} \\ a_{31} & a_{32} & a_{33} \end{bmatrix}, \quad (8)$$

Fig. 4 presents a graphical representation of each magnetic interference axes, relative to the true axes.

Because careful placement and installation of a magnetometer is important, the authors of [6] discuss common elements on a Printed Circuit Board (PCB) that cause magnetic interference.

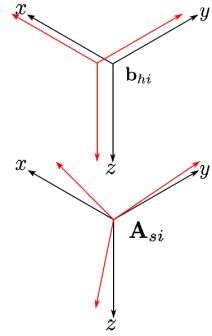


Fig. 4. Schematic representation of magnetic interferences.

V. MEASUREMENT MODEL

Combining eqns. (4) - (8), the model for the measured magnetic field $\tilde{\mathbf{h}}$ is

$$\tilde{\mathbf{h}} = \mathbf{SN}(\mathbf{A}_{si}\mathbf{h} + \mathbf{b}_{hi}) + \mathbf{b}_{so}, \quad (9)$$

where \mathbf{h} is the true magnetic field (see eqn. (2)). Note the stochastic noise is excluded from eqn. (9). While unrealistic, it simplifies the following derivations. The authors of [7] provide a good model which includes the noise.

Eqn. (9), can be re-written as

$$\tilde{\mathbf{h}} = \mathbf{Ah} + \mathbf{b} \quad (10)$$

where

$$\begin{aligned} \mathbf{A} &= \mathbf{SNA}_{si} \\ \mathbf{b} &= \mathbf{SNb}_{hi} + \mathbf{b}_{so}. \end{aligned}$$

The matrix \mathbf{A} combines scale factors, misalignments and soft-iron effects, while \mathbf{b} is the combined bias vector. It can be proved that the linear transformation of \mathbf{h} in eqn. (10) make the measurements $\tilde{\mathbf{h}}$ lie on an ellipsoid [8].

VI. CALIBRATION

The parameters \mathbf{A} and \mathbf{b} in eqn. (10) can be estimated, denoted as $\hat{\mathbf{A}}$ and $\hat{\mathbf{b}}$, such that new magnetometer measurements can be calibrated:

$$\tilde{\mathbf{h}}_c = \hat{\mathbf{A}}^{-1}(\tilde{\mathbf{h}} - \hat{\mathbf{b}}), \quad (11)$$

where $\tilde{\mathbf{h}}_c$ is the calibrated measurement.

Express \mathbf{h} , using eqn. (10),

$$\mathbf{h} = \mathbf{A}^{-1}(\tilde{\mathbf{h}} - \mathbf{b}) \quad (12)$$

Combine eqn. (12) with eqn. (3),

$$\begin{aligned} &\tilde{\mathbf{h}}^\top \mathbf{A}^{-\top} \mathbf{A}^{-1} \tilde{\mathbf{h}} \\ &- 2\tilde{\mathbf{h}}^\top \mathbf{A}^{-\top} \mathbf{A}^{-1} \mathbf{b} \\ &+ \mathbf{b}^\top \mathbf{A}^{-\top} \mathbf{A}^{-1} \mathbf{b} - \mathcal{F}^2 = 0. \end{aligned} \quad (13)$$

Eqn. (13) can be re-written in quadric form (see eqn. (23))

$$\tilde{\mathbf{h}}^\top \tilde{\mathbf{M}} \tilde{\mathbf{h}} + \tilde{\mathbf{h}}^\top \mathbf{n} + d = 0, \quad (14)$$

where

$$\tilde{\mathbf{M}} = \mathbf{A}^{-\top} \mathbf{A}^{-1} \quad (15)$$

$$\mathbf{n} = -2\mathbf{A}^{-\top} \mathbf{A}^{-1} \mathbf{b} \quad (16)$$

$$d = \mathbf{b}^\top \mathbf{A}^{-\top} \mathbf{A}^{-1} \mathbf{b} - \mathcal{F}^2. \quad (17)$$

As noted in the previous section, this quadric surface is an ellipsoid, which requires an ellipsoid fitting algorithm to provides estimates of the quadric surface parameters, $\hat{\mathbf{M}}$, $\hat{\mathbf{n}}$ and \hat{d} . The authors of [8] propose a LS fitting method which is simple to implement, and their MATLAB m-files are readily available [9]. While a nonlinear (iterated) method is preferred, a single step fit is sufficient for most sensors, as demonstrated in Section VIII-A

Using eqn. (14) and (15) - (17) with the estimated values $\hat{\mathbf{M}}$, $\hat{\mathbf{n}}$ and \hat{d} , both $\hat{\mathbf{A}}$ (or $\hat{\mathbf{A}}^{-1}$) and $\hat{\mathbf{b}}$ can be estimated.

In cases where the correct magnitude is required, \mathcal{F} must be known (see Section II) to calculate $\hat{\mathbf{A}}^{-1}$, such that

$$\hat{\mathbf{b}} = -\frac{1}{2} \hat{\mathbf{M}}^{-1} \hat{\mathbf{n}} \quad (18)$$

$$\hat{\mathbf{A}}^{-1} = \frac{\mathcal{F}}{\sqrt{\hat{\mathbf{n}}^\top \hat{\mathbf{M}}^{-1} \hat{\mathbf{n}}} - \hat{d}} \hat{\mathbf{M}}^{-\frac{1}{2}}, \quad (19)$$

where the calibrated sphere has radius \mathcal{F} . A detailed explication is provided in [7].

However, in many applications such as in attitude estimation, the magnitude is irrelevant, and the radius \mathcal{F} is typically chosen to be one, as a matter of convenience.

VII. HEADING CALCULATION

Once the magnetometer calibration values are known, the estimated tilt-compensated *magnetic heading* $\hat{\psi}$, can be determined by the following equation:

$$\hat{\psi}_m = \text{atan2}(a_1, a_2), \quad (20)$$

where

$$a_1 = -m_y \cos \hat{\phi} + m_z \sin \hat{\phi},$$

$$a_2 = m_x \cos \hat{\theta} + (m_y \sin \hat{\phi} + m_z \cos \hat{\phi}) \sin \hat{\theta}.$$

The estimated roll angle is $\hat{\phi}$, the estimated pitch angle is $\hat{\theta}$, and $\tilde{\mathbf{h}}_c = [m_x \ m_y \ m_z]^\top$.

The calculation of tilt-compensated *true heading* is

$$\hat{\psi}_t = \text{atan2}(a_1, a_2) + \mathcal{D}, \quad (21)$$

where \mathcal{D} is the correction for the local declination angle. Note, eqns. (20) and (21) use the four-quadrant tangent function (atan2). The derivation for eqn. (21) is provided in [10].

VIII. ILLUSTRATIVE EXAMPLES

A. Calibration

In Figs. 5 - 8, real data was collected from a consumer-grade magnetometer (Honeywell HMC-5883L [11]) at 50Hz in a constant-temperature lab environment. Roughly 2000 raw magnetometer samples were time stamped and stored, while the sensor was rotated first about all three axes, followed by off-axis rotations. Off-line calibration parameters (eqns. (13)-(17)) were calculated from the raw data, such that a calibrated measurement could be produced (see eqn. (11)). Fig. 5 demonstrates the isometric view of the raw data (red), calibrated data (yellow) and unit circle (blue). Due to magnetic field interference, the raw data contains both scaling and bias errors. If left uncalibrated, it is apparent from Fig. 6 that any 2D heading calculation result in errors of roughly 45°. This is because the magnetic north vector of the red ellipse points from [0, 0] to [-2, 1] instead of [0, 0] to [0, 1] as it does on the unit-circle. Both Figs. 7 and 8 show the vertical error components, which would result in 3D heading calculation errors if uncalibrated data were used.

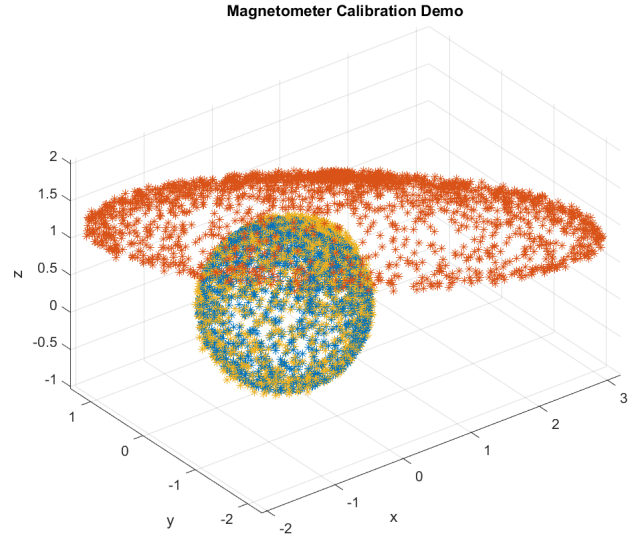


Fig. 5. Magnetometer calibration, isometric view.

B. Heading calculation

In Figs. 9 - 11, a simulated UAV climbs from sea-level to an altitude of 80m at a pitch angle of 10° (roll = 0°), then rolls 60° to turn, and orbits continuously at a 60° roll, 0° pitch. Fig. 9 demonstrates the necessity of accounting for roll and pitch angles in the calculation of the heading (see eqn. (20)), whereas Fig. 10 demonstrates the necessity of accounting for the correction from magnetic north to true north (see eqn. (21)). Fig. 11 shows the heading estimation error for a consumer-grade magnetometer (Honeywell HMC-5883L [11]) after calibration and compensation for tilt (i.e. roll and pitch angles), as well as declination angle. The apparent empty vertical region in the residuals of Figs. 10

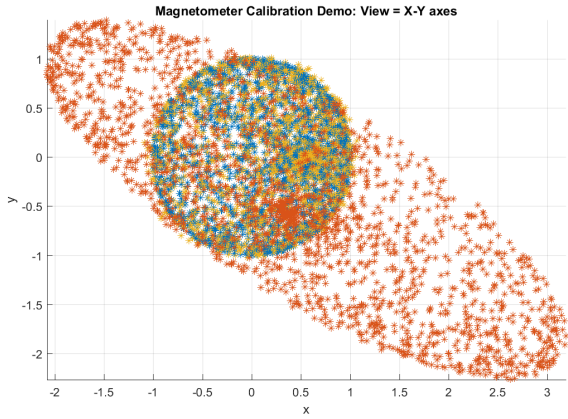


Fig. 6. Magnetometer calibration, X-Y axes view.

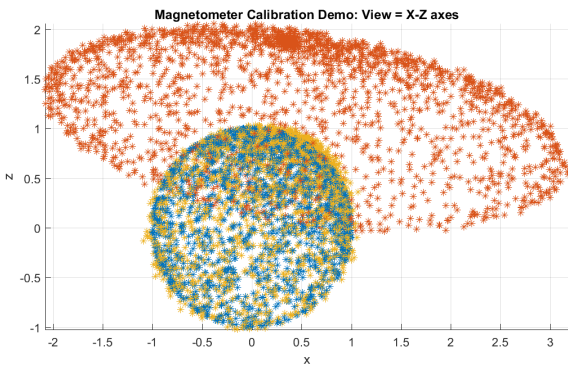


Fig. 7. Magnetometer calibration, X-Z axes view.

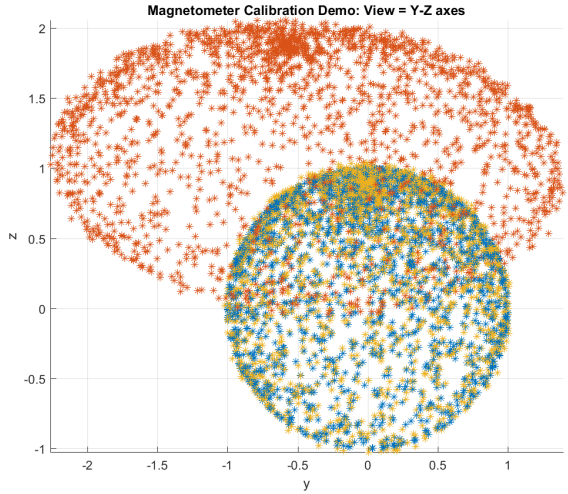


Fig. 8. Magnetometer calibration, Y-Z axes view.

and 11 (at $t = 80, 120, 150, 180, 220$) are the result of the wrap function for values between $\pm 180^\circ$. The heading accuracy of a consumer-grade magnetometer is roughly $\pm 2^\circ 1\sigma$ (see [11]); the residual plot in Fig. 11 validates the expected heading accuracy.

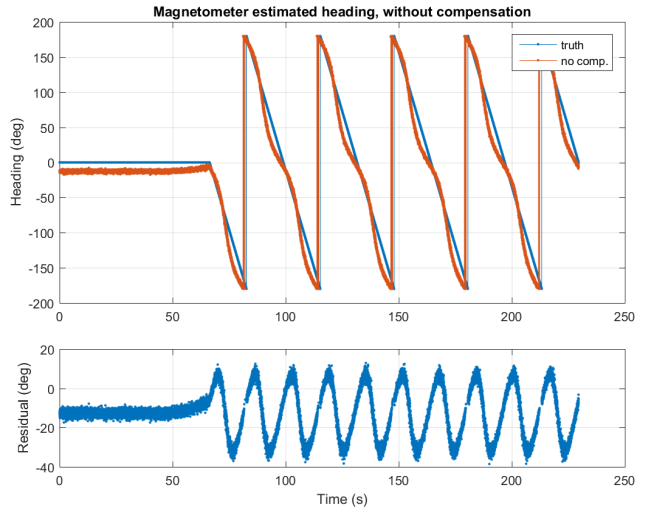


Fig. 9. Magnetometer heading estimation error without compensation.

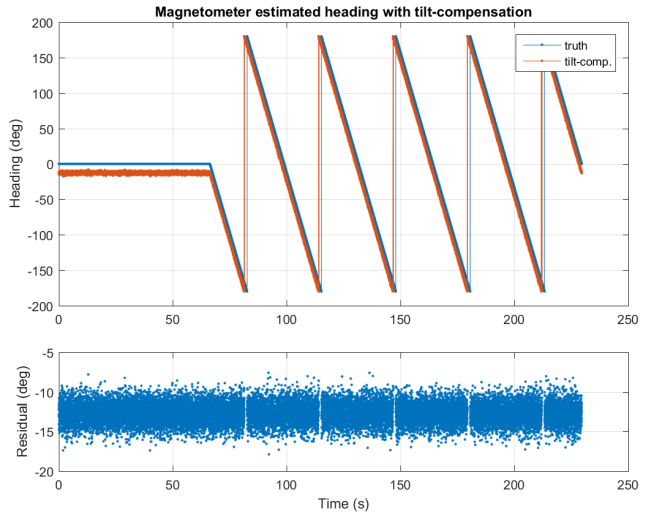


Fig. 10. Magnetometer heading estimation error, with tilt-compensation.

IX. APPENDIX

A. Quadrics

Quadrics are surfaces that can be expressed as a second-order polynomial in x , y and z . They include popular surfaces such as spheres, ellipsoids, paraboloids, etc. As we will see in Section VI, quadrics are used to fit raw magnetometer measurements to an ellipsoid. The rotation and scaling parameters of the ellipsoid are used to calibrate the raw measurements, align them on a unit-sphere and compute a magnetic heading vector.

The general implicit equation of a quadric surface \mathcal{S} is given by:

$$\begin{aligned} \mathcal{S} : & ax^2 + by^2 + cz^2 \\ & 2fyz + 2gxz + 2hxy + \\ & 2px + 2qy + 2rz + d = 0 \end{aligned} \quad (22)$$

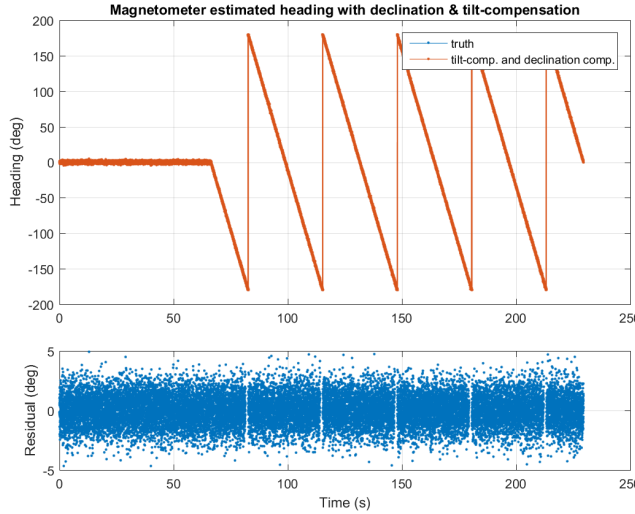


Fig. 11. Magnetometer heading estimation error, with tilt-compensation and declination angle correction.

Eqn. (22) can be written in a semi-matrix form

$$\mathbf{x}^\top \mathbf{M} \mathbf{x} + \mathbf{x}^\top \mathbf{n} + d = 0 \quad (23)$$

where \mathbf{x} is

$$\mathbf{x} = [x \ y \ z]^\top$$

and \mathbf{M} and \mathbf{n} are

$$\mathbf{M} = \begin{bmatrix} a & f & g \\ f & b & h \\ g & h & c \end{bmatrix}, \quad \mathbf{n} = \begin{bmatrix} p \\ q \\ r \end{bmatrix}.$$

A sphere of radius one, centered at origin, is defined as

$$\mathbf{M} = \begin{bmatrix} 1 & 0 & 0 \\ 0 & 1 & 0 \\ 0 & 0 & 1 \end{bmatrix}, \quad \mathbf{n} = \begin{bmatrix} 0 \\ 0 \\ 0 \end{bmatrix}, \text{ and } d = -1.$$

Eqn. (22) can also be written as

$$\mathbf{v}^\top \mathbf{Q} \mathbf{v} = 0,$$

where \mathbf{v} and \mathbf{Q} are, respectively:

$$\mathbf{v} = [x \ y \ z \ 1]^\top, \quad \mathbf{Q} = \left[\begin{array}{c|c} \mathbf{M} & \mathbf{n} \\ \hline \mathbf{n}^\top & d \end{array} \right],$$

The type of quadric is determined by the properties of the matrices \mathbf{M} and \mathbf{Q} as detailed in [12].

B. WMM

The following figures are from the US/UK World Magnetic Model - Epoch 2015, for Declination angle (Fig. 12), Total Intensity (Fig. 13), Horizontal Intensity (Fig. 14), Inclination angle (Fig. 15), as well as Magnetic Field North Component (Fig. 16), East Component (Fig. 17), and Down Component (Fig. 18).

REFERENCES

- [1] M. Kayton and W. R. Fried, *Avionics Navigation Systems*. Wiley-Interscience, 2nd Ed., 1998.
- [2] P. D. Groves, *Principles of GNSS, Inertial, and Multisensor Integrated Navigation Systems*. Artech House, 2013.
- [3] J. A. Farrell, *Aided Navigation: GPS with High Rate Sensors*. McGraw Hill, 2008.
- [4] National Oceanic and Atmospheric Administration. (2016) World Magnetic Model. [Online]. Available: <https://www.ngdc.noaa.gov/geomag/WMM/DoDWMM.shtml>
- [5] V. Renaudin, M. Afzal, and G. Lachapelle, "Complete Triaxis Magnetometer Calibration in the Magnetic Domain," *Hindawi Publishing Corporation: Journal of Sensors*, vol. 2010, 2010.
- [6] T. Ozyagcilar, "Layout Recommendations for PCBs Using a Magnetometer Sensor," Freescale Semiconductor, Application Note AN4247, November 2015.
- [7] M. Kok, J. Hol, T. Schon, F. Gustafsson, and H. Luinge, "Calibration of a magnetometer in combination with inertial sensors," *IEEE 2012 15th International Conference on Information Fusion (FUSION)*, 2012.
- [8] Q. Li and J. Griffiths, "Least Squares Ellipsoid Specific Fitting," *IEEE Proceedings of the Geometric Modeling and Processing 2004 (GMP'04)*, 2004.
- [9] Li, Q. (2016) Ellipsoid fitting. [Online]. Available: <http://www.mathworks.com/matlabcentral/fileexchange/23377-ellipsoid-fitting>
- [10] T. Ozyagcilar, "Implementing a Tilt-Compensated eCompass using Accelerometer and Magnetometer Sensors," Freescale Semiconductor, Application Note AN4248, November 2015.
- [11] Anon., "3-Axis Digital Compass IC HMC5883L," Honeywell International Inc., Datasheet HMC5883L, March 2011.
- [12] Standard Mathematical Tables and Formulas. (2016) Quadrics. [Online]. Available: <http://www.geom.uiuc.edu/docs/reference/CRC-formulas/node61.html>

US/UK World Magnetic Model - Epoch 2015.0
Main Field Declination (D)

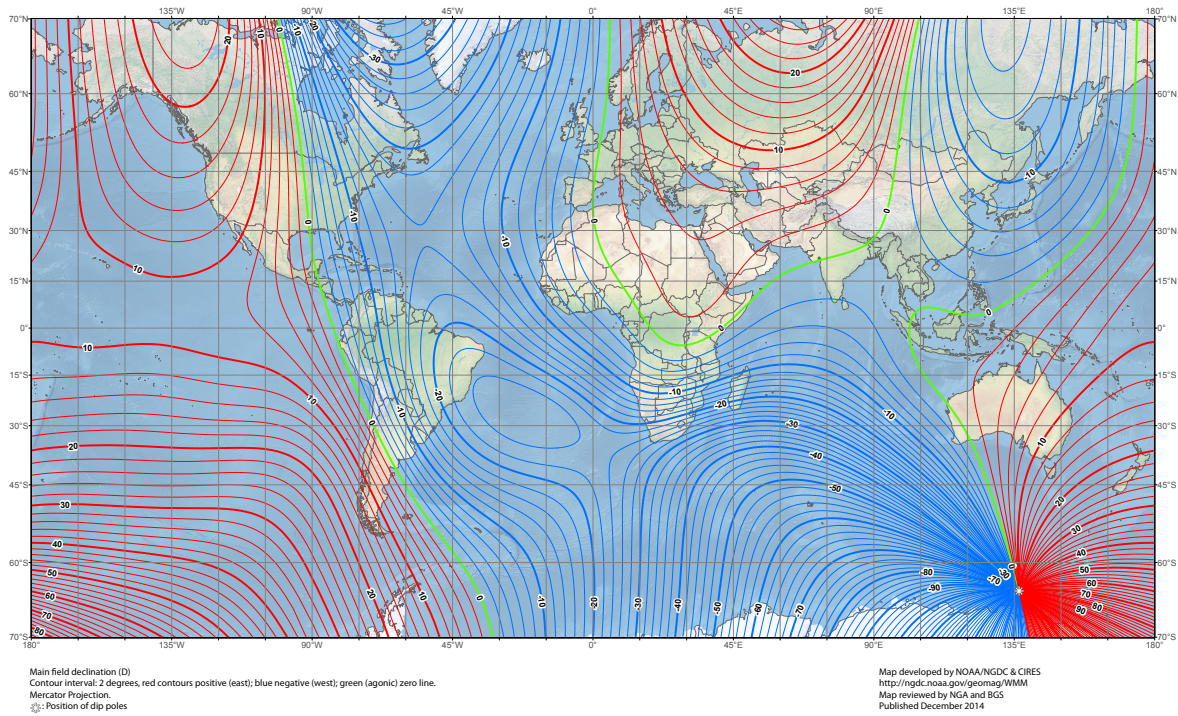


Fig. 12. US/UK World Magnetic Model - Epoch 2015, Declination angle. [4]

US/UK World Magnetic Model - Epoch 2015.0
Main Field Total Intensity (F)

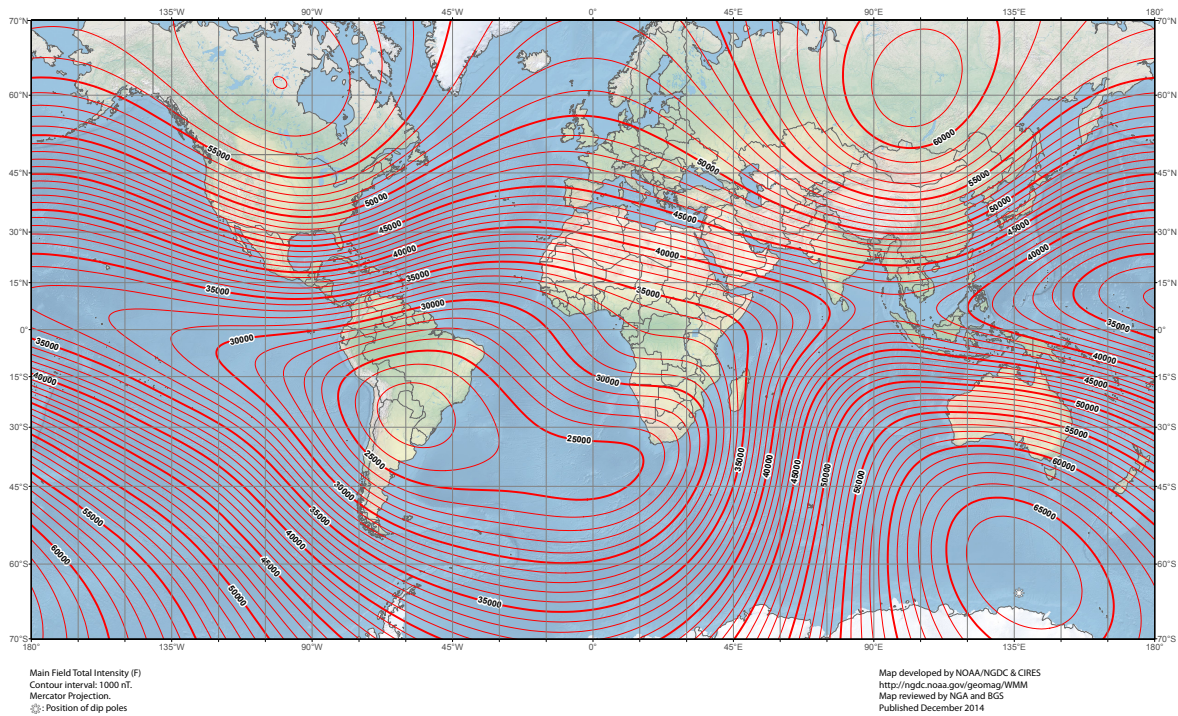


Fig. 13. US/UK World Magnetic Model - Epoch 2015, Total Intensity. [4]

US/UK World Magnetic Model - Epoch 2015.0
Main Field Horizontal Intensity (H)

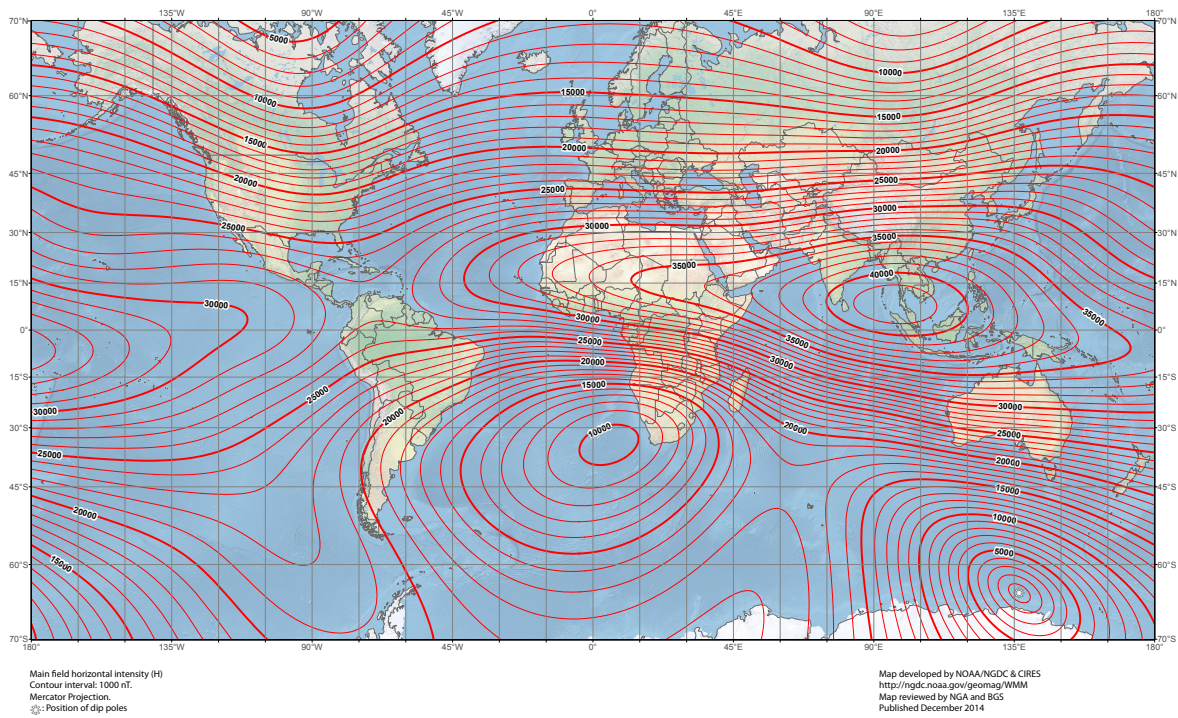


Fig. 14. US/UK World Magnetic Model - Epoch 2015, Horizontal Intensity. [4]

US/UK World Magnetic Model - Epoch 2015.0
Main Field Inclination (I)

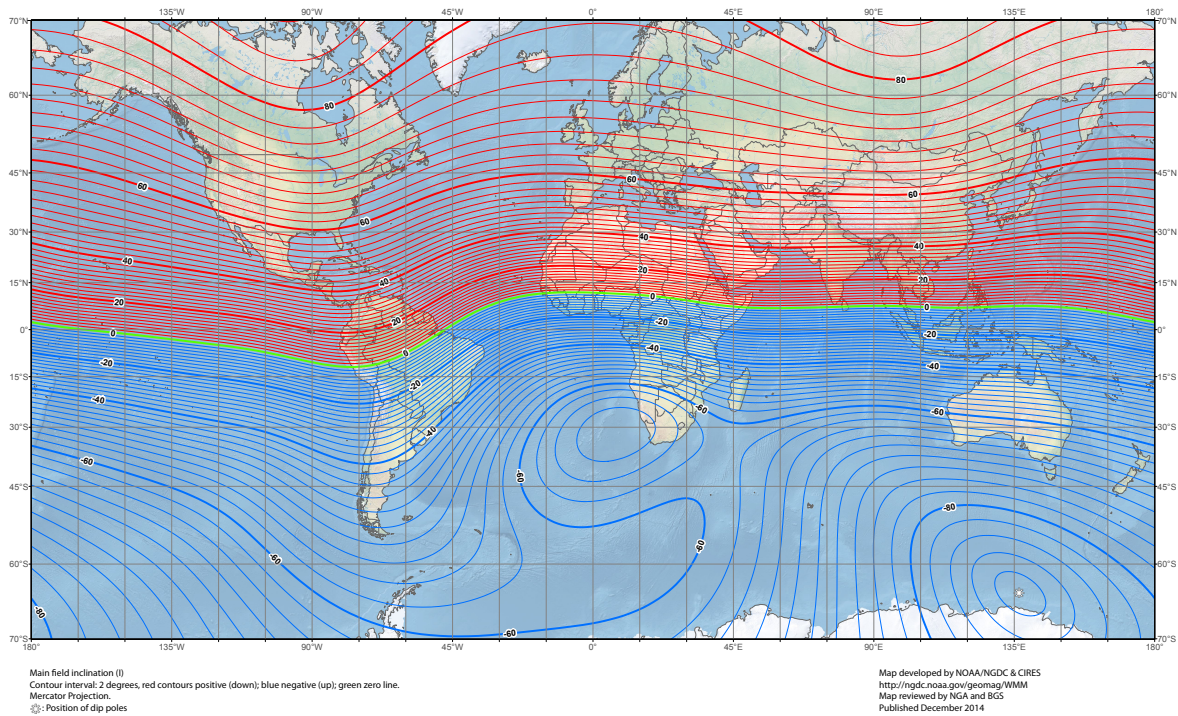


Fig. 15. US/UK World Magnetic Model - Epoch 2015, Inclination angle. [4]

US/UK World Magnetic Model - Epoch 2015.0
Main Field North Component (X)

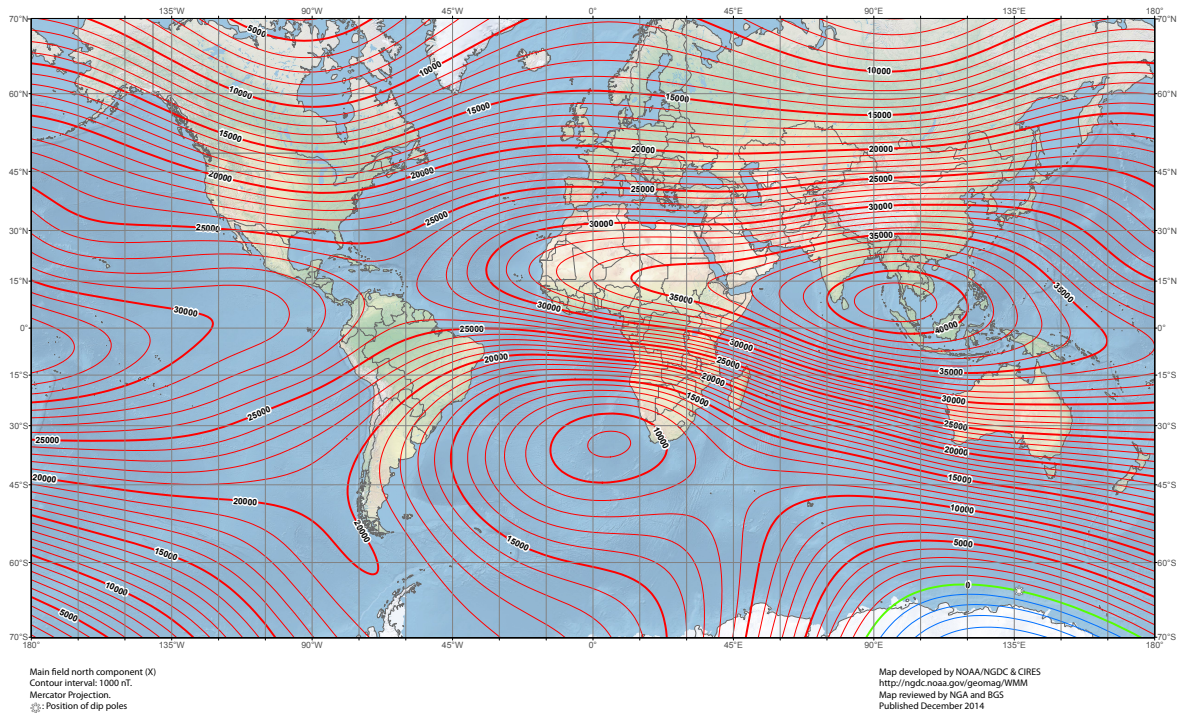


Fig. 16. US/UK World Magnetic Model - Epoch 2015, Magnetic Field North Component. [4]

US/UK World Magnetic Model - Epoch 2015.0
Main Field East Component (Y)

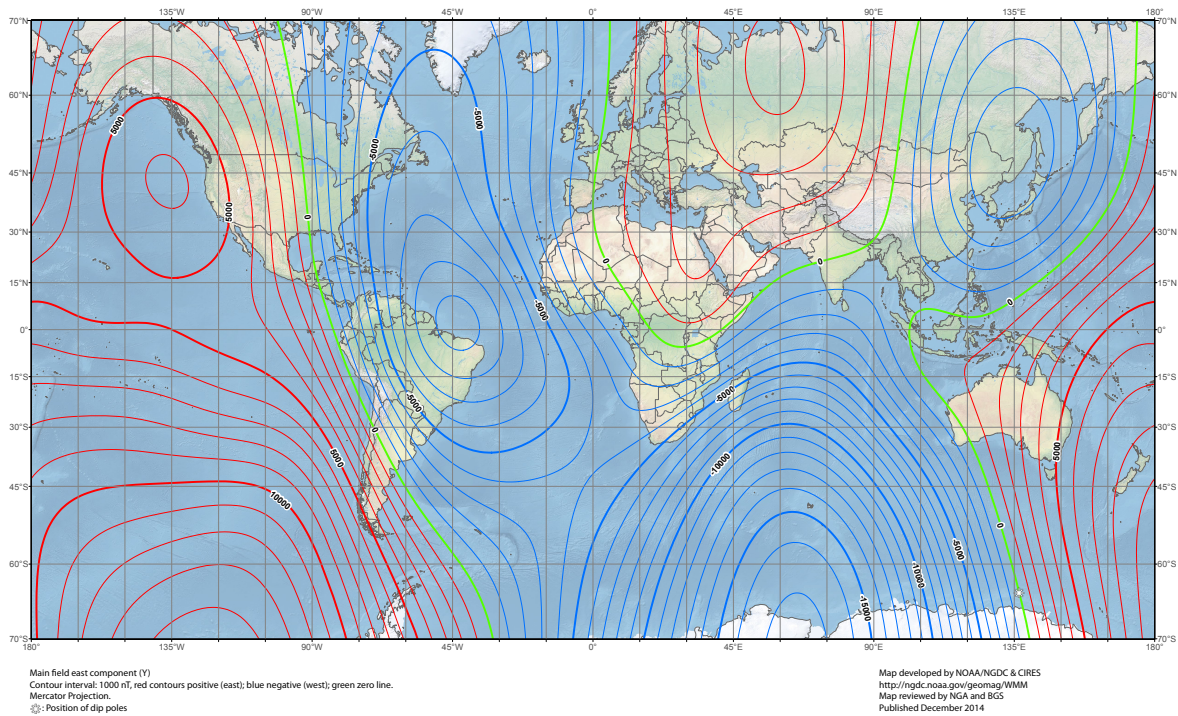


Fig. 17. US/UK World Magnetic Model - Epoch 2015, Magnetic Field East Component. [4]

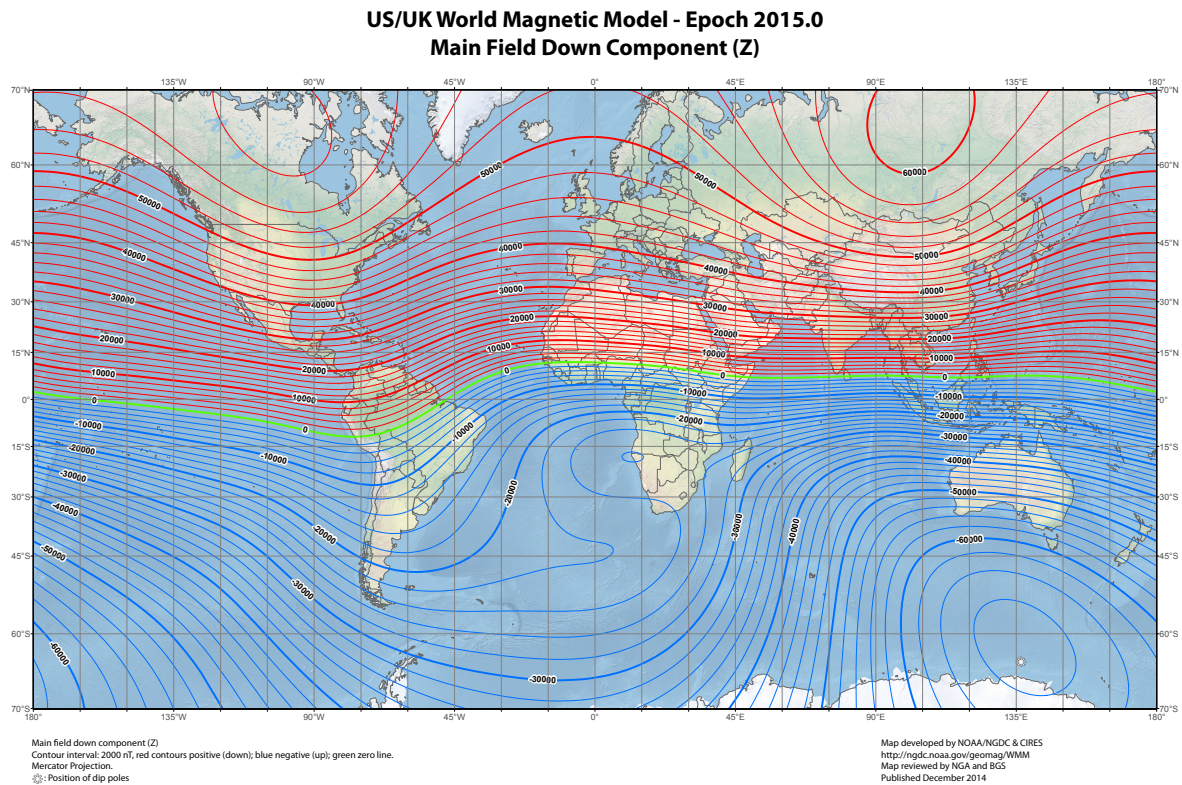


Fig. 18. US/UK World Magnetic Model - Epoch 2015, Magnetic Field Down Component. [4]